Multifractal structure of the harmonic measure of diffusion-limited aggregates

Mogens H. Jensen,[1] Anders Levermann,[2] Joachim Mathiesen,[1] and Itamar Procaccia[2]
[1]*The Niels Bohr Institute, 17 Blegdamsvej, Copenhagen, Denmark*
[2]*Department of Chemical Physics, The Weizmann Institute of Science, Rehovot 76100, Israel*
(Received 10 October 2001; published 25 March 2002)

The method of iterated conformal maps allows one to study the harmonic measure of diffusion-limited aggregates with unprecedented accuracy. We employ this method to explore the multifractal properties of the measure, including the scaling of the measure in the deepest fjords that were hitherto screened away from any numerical probing. We resolve probabilities as small as 10^{-35}, and present an accurate determination of the generalized dimensions and the spectrum of singularities. We show that the generalized dimensions D_q are infinite for $q<q^*$, where q^* is of the order of -0.2. In the language of $f(\alpha)$ this means that α_{max} is finite. The $f(\alpha)$ curve loses analyticity (the phenomenon of ''phase transition'') at α_{max} and a finite value of $f(\alpha_{max})$. We consider the geometric structure of the regions that support the lowest parts of the harmonic measure, and thus offer an explanation for the phase transition, rationalizing the value of q^* and $f(\alpha_{max})$. We thus offer a satisfactory physical picture of the scaling properties of this multifractal measure.

DOI: 10.1103/PhysRevE.65.046109 PACS number(s): 02.50.−r, 05.40.−a, 47.27.Gs, 47.27.Jv

I. INTRODUCTION

Multifractal measures are normalized distributions lying upon fractal sets. Such measures appear naturally in a variety of nonlinear physics context, the most well studied being natural measures of chaotic dynamical systems [1–3]. Other well-studied examples are the voltage distribution of random resistor networks [4,5]. In this paper, we address the harmonic measure of diffusion-limited aggregates (DLA) [6], which is the probability measure for a random walker coming from infinity to hit the boundary of the fractal cluster. This was one of the earliest multifractal measures to be studied in the physics literature [7], but the elucidation of its properties was made difficult by the extreme variation of the probability to hit the tips of a DLA versus hitting the deep fjords. With usual numerical techniques it is quite impossible to estimate accurately the extremely small probabilities to penetrate the fjords. Contrary to harmonic measures of conformally invariant fractals such as random walks and percolation clusters whose multifractal properties can be solved exactly [8,9], the present multifractal measure posed stubborn barriers to mathematical progress.

The multifractal properties of fractal measures in general, and of the harmonic measure of DLA, in particular, are conveniently studied in the context of the generalized dimensions D_q, and the associated $f(\alpha)$ function [10,11]. The simplest definition of the generalized dimensions is in terms of a uniform covering of the boundary of a DLA cluster with boxes of size ℓ, and measuring the probability for a random walker coming from infinity to hit a piece of boundary that belongs to the i'th box. Denoting this probability by $P_i(\ell)$, one considers [10]

$$D_q \equiv \lim_{\ell \to 0} \frac{1}{q-1} \frac{\ln \sum_i P_i^q(\ell)}{\ln \ell}, \tag{1}$$

where the index i runs over all the boxes that contain a piece of the boundary. The limit $D_0 \equiv \lim_{q \to 0^+} D_q$ is the fractal, or box dimension of the cluster. $D_1 \equiv \lim_{q \to 1^+} D_q$ and D_2 are the well-known information and correlation dimensions, respectively [2,12,13]. It is well established by now [11] that the existence of an interesting spectrum of values D_q is related to the probabilities $P_i(\ell)$ having a spectrum of ''singularities'' in the sense that $P_i(\ell) \sim \ell^\alpha$ with α taking on values from a range $\alpha_{\min} \leqslant \alpha \leqslant \alpha_{\max}$. The frequency of observation of a particular value of α is determined by the function $f(\alpha)$, where [with $\tau(q) \equiv (q-1)D_q$]

$$f(\alpha) = \alpha q(\alpha) - \tau[q(\alpha)], \quad \frac{\partial \tau(q)}{\partial q} = \alpha(q). \tag{2}$$

The understanding of the multifractal properties and the associated $f(\alpha)$ spectrum of DLA clusters have been a long standing issue. Of particular interest are the minimal and maximal values α_{min} and α_{max} relating to the largest and smallest growth probabilities, respectively.

The minimal value of α is relatively easy to estimate, since it is related to the scaling of the harmonic measure near the most probable tip. While the often cited Turkevich-Scher conjecture [14] that α_{min} satisfies the scaling relation $D_0 = 1 + \alpha_{min}$ is probably not exact, it comes rather close to the mark. On the other hand, the maximal value of α is a much more subtle issue. As a DLA cluster grows the large branches screen the deep fjords more and more and the probability for a random walker to get into these fjords (say around the seed of the cluster) becomes smaller and smaller. A small growth probability corresponds to a large value of α. Previous literature hardly agrees about the actual value of α_{max}. Ensemble averages of the harmonic measure of DLA clusters indicated a rather large value of $\alpha_{max} \sim 8$ [15]. In subsequent experiments on non-Newtonian fluids [16] and on viscous fingers [17], similar large values of α_{max} were also observed. These numerical and experimental indications of a very large value of α_{max} led to a conjecture that, in the limit of a large, self-similar cluster some fjords will be exponentially screened and thus causing $\alpha_{max} \to \infty$ [18].

 ©2002 The American Physical Society

If indeed $\alpha_{max}\to\infty$, this can be interpreted as a phase transition [19] (nonanalyticity) in the q dependence of D_q, at a value of q^* satisfying $q^*\geqslant 0$. If the transition takes place for a value $q^*<0$ then α_{max} is finite. Lee and Stanley [20] proposed that α_{max} diverges as $R^2/\ln R$ with R being the radius of the cluster. Schwarzer *et al.* [21] proposed that α_{max} diverges only logarithmically in the number of added particles. Blumenfeld and Aharony [22] proposed that channel-shaped fjords are important and proposed that $\alpha_{max}\sim M^x/\ln M$, where M is the mass of the cluster; Harris and Cohen [23], on the other hand, argued that straight channels might be so rare that they do not make a noticeable contribution, and α_{max} is finite, in agreement with Ball and Blumenfeld who proposed [24] that α_{max} is bounded. Obviously, the issue was not quite settled. The difficulty is that it is very hard to estimate the smallest growth probabilities using models or direct numerical simulations.

In a recent paper [25], we used the method of iterated conformal maps to offer an accurate determination of the probability for the rarest events. The main result that was announced was that α_{max} exists and the phase transition occurs at a q value that is slightly negative. In the present paper, we discuss the results in greater detail, and offer additional insights to the geometric interpretation of the phase transition. In Sec. II, we summarize briefly the method of iterated conformal maps and explain how it is employed to compute the harmonic measure of DLA with unprecedented accuracy. In Sec. III, we perform the multifractal analysis and present the calculation of the $f(\alpha)$ curve. In Sec. IV, we discuss a complementary point of view of the scaling properties of the rarest regions of the measure, to achieve in Sec. V a geometric interpretation of the phase transition. Section VI offers a short discussion.

II. ACCURATE CALCULATION OF THE HARMONIC MEASURE

A. DLA via iterated conformal maps

Consider a DLA of n particles and denote the boundary of the cluster by $z(s)$, where s is an arc-length parametrization. Invoke now a conformal map $\Phi^{(n)}(\omega)$ that maps the exterior of the unit circle in the mathematical plane ω onto the complement of the cluster of n particle in the z plane. On the unit circle $e^{i\theta}$ the harmonic measure is uniform, $P(\theta)d\theta = d\theta/2\pi$. The harmonic measure of an element ds on the cluster in the physical space is then determined as

$$P(s)ds\sim\frac{ds}{|\Phi'^{(n)}(e^{i\theta})|}, \tag{3}$$

where $\Phi^{(n)}(e^{i\theta})=z(s)$. Note that in electrostatic parlance $1/|\Phi'^{(n)}(\omega)|$ is the electric field at the position $z=\Phi^{(n)}(\omega)$. Thus, in principle, if we can have an accurate value of the conformal map $\Phi^{(n)}(\omega)$ for all values $\omega=e^{i\theta}$ we can compute the harmonic measure with desired precision. We will see that this is easier said than done, but nevertheless this is the basic principle of our approach.

We thus need to find the conformal map $\Phi^{(n)}(\omega)$. A method for this purpose was developed in a recent series of papers [26–28]. The map $\Phi^{(n)}(w)$ is made from compositions of elementary maps $\phi_{\lambda,\theta}$,

$$\Phi^{(n)}(w)=\Phi^{(n-1)}(\phi_{\lambda_n,\theta_n}(w)), \tag{4}$$

where the elementary map $\phi_{\lambda,\theta}$ transforms the unit circle to a circle with a semicircular ''bump'' of linear size $\sqrt{\lambda}$ around the point $w=e^{i\theta}$. We use below the same map $\phi_{\lambda,\theta}$ that was employed in Refs. [26–30]. With this map $\Phi^{(n)}(w)$ adds on a semicircular new bump to the image of the unit circle under $\Phi^{(n-1)}(w)$. The bumps in the z plane simulate the accreted particles in the physical space formulation of the growth process. Since we want to have *fixed size* bumps in the physical space, say of fixed area λ_0, we choose in the nth step

$$\lambda_n=\frac{\lambda_0}{|\Phi^{(n-1)'}(e^{i\theta_n})|^2}. \tag{5}$$

The recursive dynamics can be represented as iterations of the map $\phi_{\lambda_n,\theta_n}(w)$,

$$\Phi^{(n)}(w)=\phi_{\lambda_1,\theta_1}\circ\phi_{\lambda_2,\theta_2}\circ\ldots\circ\phi_{\lambda_n,\theta_n}(\omega). \tag{6}$$

It had been demonstrated before that this method represents DLA accurately, providing many analytic insights that are not available otherwise [29,30].

B. Computing the harmonic measure

In terms of computing the harmonic measure we note the close relationship between Eqs. (3) and (5). Clearly, moments of the harmonic measure can be computed from moments of λ_n. For our purpose here we quote a result established in Ref. [27], which is

$$\langle\lambda_n^q\rangle\equiv(1/2\pi)\int_0^{2\pi}\lambda_n^q(\theta)d\theta\sim n^{-2qD_{2q+1}/D}. \tag{7}$$

To compute $\tau(q)$ we rewrite this average as

$$\langle\lambda_n^q\rangle=\int ds\left|\frac{d\theta}{ds}\right|\lambda_n^q(s)=\int ds\frac{\lambda^{q+1/2}(s)}{\sqrt{\lambda_0}}, \tag{8}$$

where s is the arc length of the physical boundary of the cluster. In the last equality we used the fact that $|d\theta/ds| = \sqrt{\lambda_n/\lambda_0}$. We stress at this point that in order to measure these moments for $q\leqslant 0$ we *must* go into arc-length representation.

To make this crucial point clear we discuss briefly what happens if one attempts to compute the moments from the definition (7). Having at hand the conformal map $\Phi^{(n)}(e^{i\theta})$, one can choose randomly as many points on the unit circle $[0,2\pi]$ as one wishes, obtain as many (accurate) values of λ_n, and try to compute the integral as a finite sum. The problem is of course that using such an approach *the fjords are not resolved*. To see this we show in Fig. 1, left panel, the

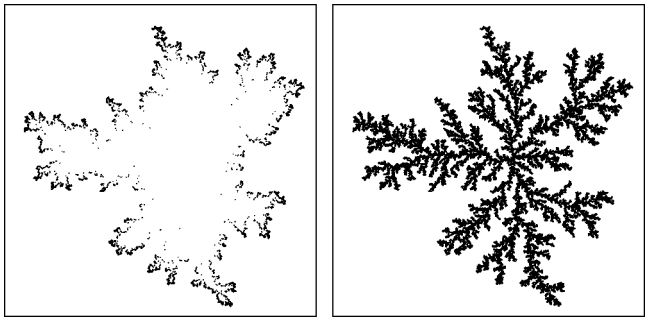

FIG. 1. Left panel, the boundary of the cluster probed by a random search with respect to the harmonic measure. Right panel, the boundary of the cluster probed by the present method.

region of a typical cluster of 50 000 particles that is being visited by a random search on the unit circle, with 50 000 samples. Like in direct simulations using random walks, the rarest events are not probed, and no serious conclusion regarding the phase transition is possible. Another method that cannot work is to try to compute $\langle \lambda_n^q \rangle$ by sampling on the arc length in a naive way. The reason is that the inverse map $[\Phi^{(n)}]^{-1}(s)$ cannot resolve θ values that belong to deep fjords. As the growth proceeds, reparametrization squeezes the θ values that map fjords into minute intervals, below the computer numerical resolution. To see this, consider the following estimate of the resolution we can achieve in the physical space:

$$\Delta\theta = \frac{\Delta s}{|\Phi^{(n)\prime}|} = \sqrt{\lambda_n}\frac{\Delta s}{\sqrt{\lambda_0}}, \tag{9}$$

or equivalently

$$\frac{\Delta s}{\sqrt{\lambda_0}} = \frac{\Delta\theta}{\sqrt{\lambda_n}}. \tag{10}$$

On the left hand side, we have the resolution in the physical space relative to the fixed linear size of the particles. With double precision numerics we can resolve values of $\Delta\theta \sim 10^{-16}$ and since we know that the values of $\lambda_{30\,000}$ can be as small as 10^{-70} inside the deepest fjords (and see below), we see that

$$\frac{\Delta s}{\sqrt{\lambda_0}} \sim \frac{10^{-16}}{10^{-35}} = 10^{19}. \tag{11}$$

Therefore, the resolution in the physcial space that is necessary to achieve a meaningful probe of the deep fjord is highly inappropriate.

The bottom line is that to compute the values of $\lambda_n(s)$ effectively we must use the full power of our iterated conformal dynamics, carrying the history with us, to iterate forward and backward at will to resolve accurately the θ and λ_n values associated with any given particle on the fully grown cluster.

To do this we recognize that every time we grow a semicircular bump we generate two new branch cuts in the map

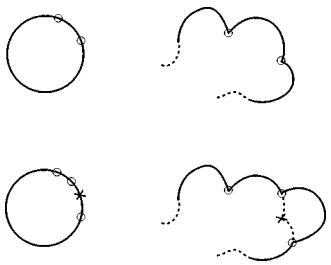

FIG. 2. A typical growth process in which an existing branch cut is "buried" under the new bump. Such events reduce the number of branch cuts below $2n$, with n being the number of particles.

$\Phi^{(n)}$. We find the position on the boundary between every two branch cuts, and there compute the value of λ_n. The first step in our algorithm is to generate the location of these points intermediate to the branch cuts [31]. Each branch cut has a preimage on the unit circle that will be indexed with three indices, $w_{j,\ell}^{k(\ell)} \equiv \exp[i\theta_{j,\ell}^{k(\ell)}]$. The index j represents the generation when the branch cut was created (i.e., when the jth particle was grown). The index ℓ stands for the generation at which the analysis is being done (i.e., when the cluster has ℓ particles). The index k represents the position of the branch cut along the arc length, and it is a function of the generation ℓ. Note that if two branch cuts belonging to the same bump are exposed, they get two consecutive indices. Since bumps may overlap during growth, branch cuts are then covered, cf. Fig. 2. Therefore, the maximal $k, k_{max} \leqslant 2\ell$. After each iteration the preimage of each branch cut moves on the unit circle, but its physical position remains. This leads to the equation that relates the indices of a still exposed branch cut that was created at generation j to a later generation n,

$$\begin{aligned}\Phi^{(n)}(w_{j,n}^{k(n)}) &\equiv \Phi^{(n)}(\phi^{-1}_{\lambda_n,\theta_n} \circ \ldots \circ \phi^{-1}_{\lambda_{j+1},\theta_{j+1}}(w_{j,j}^{\tilde{k}(j)})) \\ &= \Phi^{(j)}(w_{j,j}^{\tilde{k}(j)}).\end{aligned} \tag{12}$$

Note that the sorting indices $\tilde{k}(j)$ are not simply related to $k(n)$, and need to be tracked as follows. Suppose that the list $w_{j,n-1}^{k(n-1)}$ is available. In the nth generation we choose randomly a new θ_n, and find two new branch cuts that on the unit circle are at angles $\theta_n^{\pm}$. If one (or very rarely more) branch cut of the updated list $\phi^{-1}_{\lambda_n,\theta_n}(w_{j,n-1}^{k(n-1)})$ is covered, it is eliminated from the list, and together with the sorted new pair we make the list $w_{j,n}^{k(n)}$.

Next, let us find the midpositions at which we want to compute the value of λ_n. Having a cluster of n particles we now consider all neighboring pairs of preimages $w_{j,n}^{k(n)}$ and $w_{J,n}^{k(n)+1}$ that very well may have been created at two different generations j and J. The larger of these indices (J without loss of generality) determines the generation of the intermediate position at which we want to compute the field. We want to find the preimage $u_{J,J}^{k(n)}$ of this midpoint on the unit circle, to compute $\lambda_{k(n)}$ there accurately. Using definition (12) we find the preimage

$$\arg(u_{J,J}^{k(n)}) = [\arg(w_{j,J}^{\tilde{k}(J)}) + \arg(w_{J,J}^{\tilde{k}(J)+1})]/2. \quad (13)$$

In Fig. 1, right panel, we show, for the same cluster of 50 000, the map $\Phi^{(J)}(u_{J,J}^{k(n)})$ with $k(n)$ running between 1 and k_{max}, with J being the corresponding generation of creation of the midpoint. We see that now all the particles are probed, and every single value of $\lambda_{k(n)}$ can be computed.

To compute these $\lambda_{k(n)}$ accurately, we define [in analogy to Eq. (12)] for every $J<m\leqslant n$,

$$u_{J,m}^{k(n)} \equiv \phi_{\lambda_m,\theta_m}^{-1} \circ \cdots \circ \phi_{\lambda_{j+1},\theta_{j+1}}^{-1}(u_{J,J}^{k(n)}). \quad (14)$$

Finally, $\lambda_{k(n)}$ is computed from the definition (5) with

$$\Phi^{(n)\prime}(u_{J,n}^{k(n)}) = \phi'_{\lambda_n,\theta_n}(u_{J,n}^{k(n)}) \cdots \phi'_{\lambda_{J+1},\theta_{J+1}}(u_{J,J+1}^{k(n)}) \times \Phi^{(J)\prime}(u_{J,J}^{k(n)}). \quad (15)$$

We wish to emphasize the relevance of this equation: the problem with the coarse resolution that was exposed by Eq. (11) occurs only inside the deepest fjords. We note, however, that the particles inside the deep fjords were deposited when the clusters were still very small. For small clusters the resolution of the fjords does not pose a difficult problem. Therefore, when we evaluate the derivative $\Phi^{(n)}$ inside the deepest fjord at a point $u_{J,n}^{k(n)}$, we make use of the fact that $J\ll n$ and write the derivative in the form

$$\Phi^{(n)\prime}(u_{J,n}^{k(n)}) = \Phi^{(J)\prime}(u_{J,J}^{k(n)}) \cdot \delta, \quad (16)$$

where δ refers to correcting terms. On the left hand side of Eq. (15) we see that within our limited numerical resolution $u_{J,n}^{k(n)}$, $u_{J,n}^{k(n)+1}$ and the correponding values of λ_n are almost identical whereas for the right hand side (RHS) this is not the case. By keeping track of the branch cuts we improve the precision inside the fjords dramatically. In other words, the large screening inside the fjords is simultaneously the problem and the solution. The problem is that we cannot use the standard approach in evaluating $\Phi^{(n)\prime}$. The solution is that for a point $u_{J,n}^{k(n)}$ inside the deepest fjords we always have that $J\ll n$ and therefore the evaluation (15) helps to improve the resolution.

In summary, the calculation is optimally accurate since we avoid as much as possible the effects of the rapid shrinking of low probability regions on the unit circle. Each derivative in Eq. (15) is computed using information from a generation in which points on the unit circle are optimally resolved.

The integral (8) is then estimated as the finite sum $\sqrt{\lambda_0}\Sigma_{k(n)}\lambda_{k(n)}^q$. We should stress that for clusters of the order of 30 000 particles we already compute, using this algorithm, $\lambda_{k(n)}$ values of the order of 10^{-70}. To find the equivalent small probabilities using random walks would require about 10^{35} attempts to see them just once. This is of course impossible, explaining the lasting confusion about the issue of the phase transition in this problem. This also means that all the $f(\alpha)$ curves that were computed before [15,32] did not converge. Note that in our calculation the small values of $\lambda_{k(n)}$ are obtained from multiplication rather than addition, and therefore can be trusted.

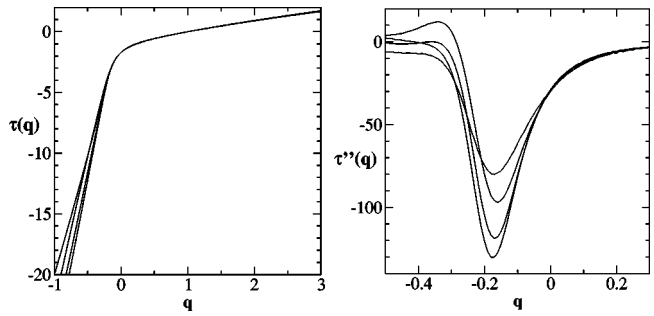

FIG. 3. Left panel, the calculated function $\tau(q)$ using clusters of n and $\overline{n}$ particles, with $n=5000$, 10 000, 15 000, and 25 000 and $\overline{n}=10\,000$, 15 000, 25 000, and 30 000, respectively. Right panel, the second derivative of $\tau(q)$ with respect to q. The minima of the curves get deeper when n is increased.

III. MULTIFRACAL ANALYSIS OF THE HARMONINC MEASURE

Having the accurate values $\lambda_{k(n)}$ we can now compute the moments (7). Since the scaling form on the RHS includes unknown coefficients, we compute the values of $\tau(q)$ by dividing $\langle\lambda_n^q\rangle$ by $\langle\lambda_{\overline{n}}^q\rangle$, estimating

$$\tau(q) \approx -D\frac{\ln\langle\lambda_n^q\rangle - \ln\langle\lambda_{\overline{n}}^q\rangle}{\ln n - \ln\overline{n}}. \quad (17)$$

Results for $\tau(q)$ for increasing values of n and $\overline{n}$ are shown in Fig. 3, left panel. It is seen that the value of $\tau(q)$ appears to grow without bound for q negative. The existence of a phase transition is however best indicated by measuring the derivatives of $\tau(q)$ with respect to q. In Fig. 3 right panel, we show the second derivative, indicating a phase transition at a value of q that recedes *away* from $q=0$ when n increases. Due to the high accuracy of our measurement of λ we can estimate already with clusters as small as 20–30 000 the q value of the phase transition as $q^*=-0.18\pm0.04$. It is quite possible that larger clusters would have indicated slighly more negative values of q^* (and see below the results of different methods of estimates), but we believe that this value is close to convergence. The fact that this is so can be seen from the $f(\alpha)$ curve that is plotted in Fig. 4. A test of convergence is that the slope of this function where it becomes essentially linear must agree with the q value of the phase transition. The straight line shown in Fig. 3 has the slope of -0.18, and it indeed approximates very accurately the slope of the $f(\alpha)$ curve where it stops being analytic. The reader should also note that the peak of the curve agrees with $D\approx1.71$, as well as the fact that $\tau(3)$ is also D as expected in this problem. The value of α_{max} is close to 20, which is higher than anything predicted before. It is nevertheless finite. We believe that this function is well converged, in contradistinction with past calculations.

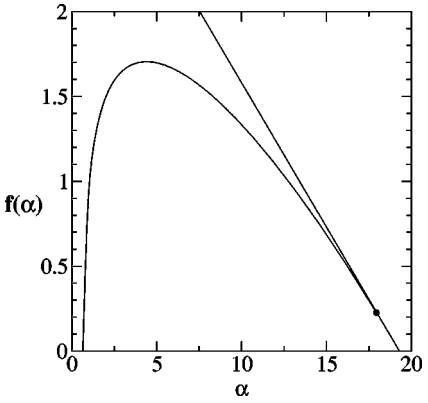

FIG. 4. Calculated function $f(\alpha)$ using $\tau(q)$ calculated from a cluster with $n=30\,000$ particles. This $f(\alpha)$ is almost indistinguishable from the one computed with $n=25\,000$ particles. We propose that this function is well converged. The black dot denotes where the curve ends, being tangent to the line with slope -0.18.

IV. ALTERNATIVE WAY TO APPROACH THE PHASE TRANSITION

An alternative way to the multifractal analysis is obtained by first reordering all the computed values of $\lambda_{k(n)}$ in ascending order. In other words, we write them as a sequence $\{\lambda_n(i)\}_{i\in I}$, where I is an ordering of the indices such that $\lambda_n(i)\leqslant\lambda_n(j)$ if $i<j$. The number of samples we consider is usually large and therefore the discrete index i/N might be treated as a continuous index $0\leqslant x\leqslant 1$ and λ_n as a nondecreasing function of x,

$$\lambda_n \equiv g(x). \tag{18}$$

We next consider the distribution of $p(\lambda_n)$, which is calculated by the usual transformation formula

$$p(\lambda_n)\sim \int \delta[\lambda_n - g(x)]dx = \frac{1}{|g'[x(\lambda_n)]|}. \tag{19}$$

Using the distribution of λ_n, we now do the following rewritings:

$$\int_0^{2\pi} \lambda_n^q d\theta = \int_0^L \lambda_n^q \frac{d\theta}{ds} ds \sim \int_0^L \lambda_n^{q+1/2} ds \tag{20}$$

$$\sim \int_0^\infty \lambda_n^{q+1/2} p(\lambda_n) d\lambda_n . \tag{21}$$

In Fig. 5, we will show that our function $g(x)$ obeys a power law for low values of x,

$$g(x)\sim x^\beta \quad \text{for } x\ll 1. \tag{22}$$

This in turn implies a power-law dependence of $p(\lambda_n)$ on λ_n

$$p(\lambda_n)\sim \frac{1}{[x(\lambda_n)]^{\beta-1}} \sim \lambda_n^{(1-\beta)/\beta} \quad \text{for } \lambda_n \ll 1. \tag{23}$$

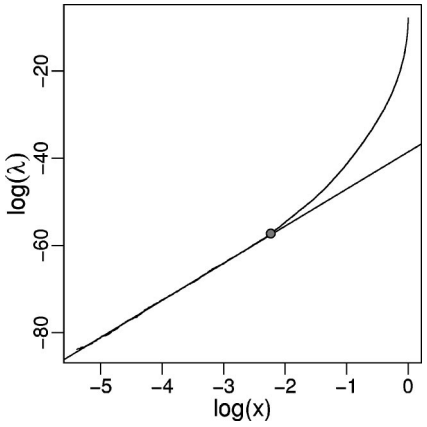

FIG. 5. Values of λ_n sorted in ascending order with respect to the variable $x=i/N$. This function is a pure power law for values of $\ln x$ smaller than the position of the circle. The power law is characterized by an exponent $\beta\approx 8.55$. This is consistent with a phase transition for $q^*\approx -0.23$.

This power-law tail means that the moment integral (21) diverges for values of q below a critical value q_c given by

$$q_c + \frac{1}{2} + \frac{1-\beta}{\beta} = -1. \tag{24}$$

Thus, $q_c = -1/2 - 1/\beta$. From Eq. (7) we see that the value of q^* satisfied the relation

$$q^* = 2q_c + 1 = -2/\beta. \tag{25}$$

In Fig. 5, we show how the values of λ_n depend on x for small values of x. The data are taken from a cluster with $n=20\,000$. Denoting the value of λ_n that is marked as a full circle by λ_c, the figure supports the existence of the power law (22) for values of λ_n smaller than λ_c. Needless to say this also implies that $p(\lambda_n)$ scales according to Eq. (23). By averaging over 16 clusters of size $n=20\,000$, we estimate the slope in Fig. 5 to be $\beta\approx 8.55$ or

$$q^* = -0.23 \pm 0.05. \tag{26}$$

Obviously, this result is in agreement with our direct calculation in Sec. III.

V. GEOMETRICAL INTERPRETATION OF THE PHASE TRANSITION

At this point we would like to interpret the origin of the phase transition, which in light of the last section stems from the power-law behavior of $p(\lambda_n)$ for small values of λ_n. We first identify the region on the cluster that supports the low values of λ_n that belong to the power-law tail of $p(\lambda_n)$.

Consider again Fig. 5. The point denoted above as λ_c defines the maximum value for which we see a power law in λ_n vs x. Therefore, the set responsible for the phase transition is the union of bumps with a value of λ_n for which $\lambda_n < \lambda_c$. This set is referred to below as the "critical set," and is shown in Fig. 6, both on the background of the rest of the cluster, and as an isolated set. This figure suggests a geomet-

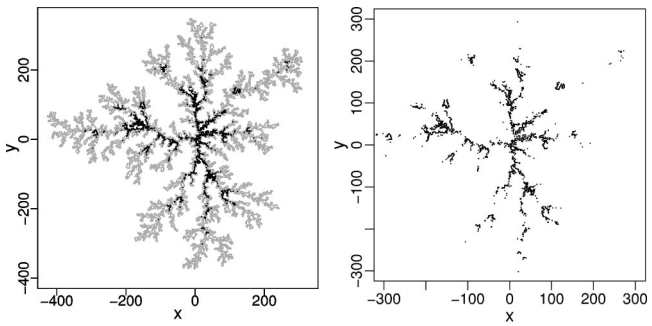

FIG. 6. Set of all particles that are associated with values of λ_n belonging to the power-law region shown in Fig. 5. In the left panel, we show the set on the background of the cluster in gray; and in the right panel, the set isolated from the rest of the cluster.

ric interpretation: the fjords in the figure all seem to have a characteristic angle. We will try first to confirm this impression using careful numerics.

Clearly, the set has several fjords; we consider them individually. Figure 7 shows an example of such a fjord. For each fjord we find the point with the minimum probability and use this for defining the bottom (or deepest point). Second, from the inside, we move to the two adjacent points which together with the deepest point define an angle. This angle is recorded, and we move to the next pair of points, and so on until the value of λ_n exceeds λ_c. Figure 7, right panel shows how the angle varies with the number of steps k. For most of the fjords considered the angle is quite large for a small number of steps (up to 3 to 4 steps). As more steps are taken the angle settles on a characteristic value around which it fluctuates. For a larger number of steps we reach the outer parts of the fjord and the angle does no longer reflect the geometry inside the fjord. The dependence of the angle on k as shown in Fig. 7 is typical for all the fjords of the set causing the phase transition and therefore we see a peak in the distribution of all the measured angles. This peak identifies an angle that is characteristic to the fjords. Figure 8 is the distribution of such typical angles over one cluster. We determine the characteristic angle, say γ_c by locating the maximum of the distribution. Finally, we calculated the average of the charateristic angle γ_c over 15 clusters of size n $=20\,000$. On the basis of that we determine the angle to be

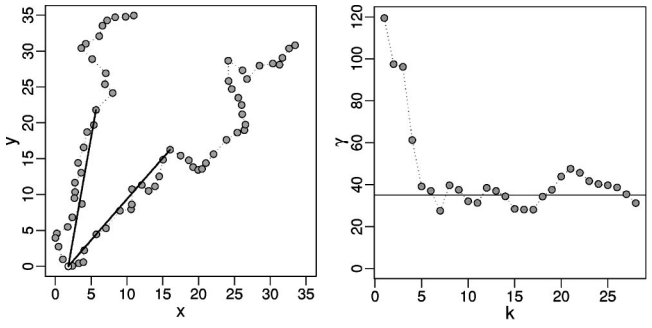

FIG. 7. Left panel, a typical deep fjord resolved on the scale of the particles. From the deepest particle the angle is computed as explained in the text. Right panel, the change of the measured angle γ as a function of the number of steps k away from the deepest particle. The angle settles on a value that depends only weakly on k.

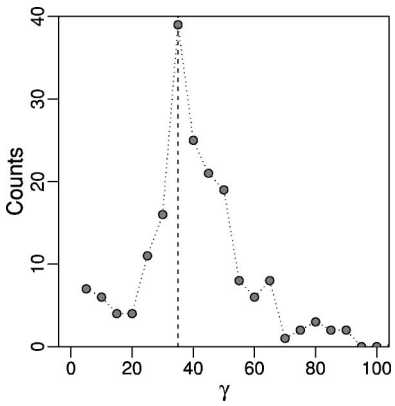

FIG. 8. Distribution of angles γ as determined by the procedure exemplified in Fig. 7 over the set shown in Fig. 6.

$$\gamma_c = 35° \pm 6°. \tag{27}$$

Finally, we can offer a geometrical model to interpret the phase transition. The results presented in this section indicate that to a reasonable approximation the least accessible fjords can be modeled as a wedge of included angle γ_c. In the Appendix, we compute the power law expected for $p(\lambda_n)$ for a wedge. The final result is

$$p(\lambda_n) \sim \lambda_n^{-(2\eta-3)/2(\eta-1)}, \tag{28}$$

where $\gamma_c = \pi/\eta$. Using our numerical result for γ_c and Eq. (25) we predict finally $q^* = -0.24 \pm 0.05$. Obviously, this is in agreement with the previous findings.

In addition, we should comment on the interpretation of $f(\alpha_{max})$ that is the value of the $f(\alpha)$ curve at the point of loss of analyticity. Within the wedge model offered here, this must be the fractal dimension of the set of wedges that support the scaling law (28). We have attempted to determine this dimension numerically by counting the number of fjords in the critical set shown in Fig. 7 as a function of the number of paricles n in the cluster. While the result of such a calculation is consistent with the proposition, the available statistics is not sufficient to establish it firmly. We thus conclude with the proposition as a conjecture, i.e., that $f(\alpha_{max})$ can be interpreted as the dimension of the set of fjords that belong to the critical set.

VI. CONCLUDING REMARKS

In conclusion, we have used the method of iterated conformal maps to compute accurately the harmonic measure of DLA clusters of moderate size. We have explained that we must use the full power of the method in order to overcome the strong contraction of the regions on the unit circle that belong to the deep fjords. By iterating back and forth, using the fact that we own the history of the iteration scheme, we could resolve probabilities as small as 10^{-35}. Using this data we could establish beyond doubt that the generalized dimensions [or, equivlently, the $f(\alpha)$ function] lose analyticity at a negative value of q, implying the existence of α_{max}. In order to understand the loss of analyticity, we offer a geometric

picture. We identified the critical set on the cluster as having harmonic probabilities that belong to the power-law tail of $p(\lambda_n)$. Considering this set we identified fjords that can be modeled as wedges of characteristic angle. Taking such wedges as a model for the fjords of the critical set, we found a value of q^* that is very close to the one computed using other methods. We thus propose that the point of nonanalyticity can be interpreted as resulting from the power-law dependence of the harmonic measure in the fjords belonging to the critical set.

ACKNOWLEDGMENTS

This work has been supported in part by the Petroleum Research Fund, The European Commission under the TMR program, and the Naftali and Anna Backenroth-Bronicki Fund for Research in Chaos and Complexity. A. L. is supported by of the Minerva Foundation, Munich, Germany.

APPENDIX: WEDGE MODEL FOR THE FJORDS OF THE CRITICAL SET

1. The conformal map and the electric field

The conformal function

$$\chi(w)=\left(i\frac{w+1}{w-1}\right)^{1/\eta} \tag{A1}$$

maps the outside of the unit circle to the inside of a wedge with opening angle $\gamma_c=\pi/\eta$, where $\eta\geqslant 1$ allows γ_c be vary between 0 and π. To calculate the electric field E, we need the inverse of χ:

$$\chi^{-1}(z)=\frac{z^{\eta}+i}{z^{\eta}-i}. \tag{A2}$$

From here we see that $\chi^{-1}(0)=-1$ and

$$\Phi^{-1}(\rho\exp[i\pi(1\pm 1)/2\eta])\rightarrow 1 \quad \text{as} \quad \rho\rightarrow\infty. \tag{A3}$$

Thus, the unit circle is unfolded onto the wedge; shifting the point $w=-1$ to the origin $z=0$; and rotating and stretching the upper half circle onto the real axis and the lower half circle to the other ray of the wedge $\rho e^{i\pi/\eta}$. The electric field follows from its definition

$$E(z)=\left|\frac{d}{dz}\ln[\chi^{-1}(z)]\right|=\frac{2\eta}{|z|}\frac{1}{|z^{\eta}+z^{-\eta}|}. \tag{A4}$$

On the real axis close to the center $z=0$, i.e., for $z=\rho\ll 1$ it becomes

$$E(\rho)=\frac{2\eta}{\rho}\frac{1}{\rho^{\eta}+\rho^{-\eta}}\approx 2\eta\rho^{\eta-1} \quad \text{for} \quad \rho\ll 1, \tag{A5}$$

while for large ρ is goes like

$$E(\rho)=\frac{2\eta}{\rho}\frac{1}{\rho^{\eta}+\rho^{-\eta}}\approx 2\eta\rho^{-(\eta+1)} \quad \text{for} \quad \rho\gg 1. \tag{A6}$$

Exactly the same relations hold for the upper ray.

2. The probability measure for λ_n

The linear size of the particles in mathematical space $\sqrt{\lambda_n}$ is proportional to the electric field,

$$\sqrt{\lambda_n}(\theta)=\sqrt{\lambda_0}E(\Phi(e^{i\theta})). \tag{A7}$$

Thus, the probability measure of the λ_n is directly related to the probability measure of the electric field. Since E is the same for the two rays of the wedge, it is sufficient to consider it only on the real axis. Starting from the uniform distribution of the θ values in mathematical space, it follows:

$$\begin{aligned}1&=\frac{dP(\theta)}{d\theta}=\frac{dP(E)}{dE}\left|\frac{dE}{d\rho}\right|\left|\frac{d\rho}{d\theta}\right|\\&=\frac{dP}{dE}\left|\frac{dE}{d\rho}\right|\left|-i\frac{d}{d\rho}\ln[\Phi^{-1}(\rho)]\right|^{-1}\\&=\frac{dP}{dE}\left|\frac{dE}{d\rho}\right|E^{-1}\end{aligned} \tag{A8}$$

or

$$dP(E)\sim\left|\frac{dE}{d\rho}(\rho)\right|^{-1}E\,dE. \tag{A9}$$

The derivative of the electric field follows from (A5) or (A6),

$$\left|\frac{dE}{d\rho}(\rho)\right|=\frac{2\eta}{\rho^2}\frac{|(\eta+1)\rho^{\eta}-(\eta-1)\rho^{-\eta}|}{(\rho^{\eta}+\rho^{-\eta})^2}, \tag{A10}$$

yielding

$$dP(E)\sim\frac{\rho(\rho^{\eta}+\rho^{-\eta})}{|(\eta+1)\rho^{\eta}-(\eta-1)\rho^{-\eta}|}dE. \tag{A11}$$

For small ρ corresponding to a small field and thus small $\sqrt{\lambda_n}$ we get

$$dP(E)\sim\rho dE\sim E^{1/(\eta-1)} \tag{A12}$$

or

$$dP(\sqrt{\lambda_n})\sim\sqrt{\lambda_n}^{-1/(\eta-1)}d\sqrt{\lambda_n}. \tag{A13}$$

For the probability density of λ_n this means

$$dP(\lambda_n)=\frac{dP(\sqrt{\lambda_n})}{d\sqrt{\lambda_n}}\frac{d\lambda_n}{2\sqrt{\lambda_n}} \tag{A14}$$

$$\sim\lambda_n^{-(2\eta-3)/2(\eta-1)}d\lambda_n. \tag{A15}$$

[1] D. Ruelle, *Statistical Mechanics, Thermodynamic Formalism* (Addison- Wesley, Reading, MA, 1978).
[2] P. Grassberger and I. Procaccia, Phys. Rev. Lett. **50**, 346 (1983).
[3] J.-P. Eckmann and D. Ruelle, Rev. Mod. Phys. **57**, 617 (1985).
[4] R. Rammal, C. Tannous, P. Breton, and A.-M.S. Tremblay, Phys. Rev. Lett. **54**, 1718 (1985).
[5] L. de Arcangelis, S. Redner, and A. Coniglio, Phys. Rev. B **31**, 4725 (1985).
[6] T.A. Witten and L.M. Sander, Phys. Rev. Lett. **47**, 1400 (1981).
[7] T.C. Halsey, P. Meakin, and I. Procaccia, Phys. Rev. Lett. **56**, 854 (1986).
[8] B. Duplantier, Phys. Rev. Lett. **84**, 1363 (2000).
[9] M. Hastings, Phys. Rev. Lett. **88**, 055506 (2002); e-print cond-mat/0109304.
[10] H.G.E. Hentschel and I. Procaccia, Physica D **8**, 435 (1983).
[11] T.C. Halsey, M.H. Jensen, L.P. Kadanoff, I. Procaccia, and B.I. Shraiman, Phys. Rev. A **33**, 1141 (1986).
[12] J. Balatoni and A. Renyi, Publ. Math. (Debrecen) **1**, 9 (1956).
[13] J.D. Farmer, Physica (Utrecht) **4D**, 366 (1982).
[14] L.A. Turkevich and H. Scher, Phys. Rev. Lett. **55**, 1026 (1985).
[15] C. Amitrano, A. Coniglio, and F. di Liberto, Phys. Rev. Lett. **57**, 1016 (1986).
[16] J. Nittmann, H.E. Stanley, E. Touboul, and G. Daccord, Phys. Rev. Lett. **58**, 619 (1987). In this paper, the viscous fingering pattern was digitized and the harmonic measure was then calculated. There was no direct measurement of the harmonic measure.
[17] K.J. Måløy, F. Boger, J. Feder, and T. Jøssang, in *Time-Dependent Effects in Disordered Materials*, edited by R. Pynn and T. Riste (Plenum, New York, 1987), p. 111.
[18] T. Bohr, P. Cvitanović, and M.H. Jensen, Europhys. Lett. **6**, 445 (1988).
[19] P. Cvitanović, in *Proceedings of the XIV Colloquium on Group Theoretical Methods in Physics*, edited by R. Gilmore (World Scientific, Singapore, 1987); in *Non-Linear Evolution and Chaotic Phenomena*, edited by P. Zweifel, G. Gallavotti, and M. Anile (Plenum, New York, 1988).
[20] J. Lee and H.E. Stanley, Phys. Rev. Lett. **61**, 2945 (1988).
[21] S. Schwarzer, J. Lee, A. Bunde, S. Havlin, H.E. Roman, and H.E. Stanley, Phys. Rev. Lett. **65**, 603 (1990).
[22] R. Blumenfeld and A. Aharony, Phys. Rev. Lett. **62**, 2977 (1989).
[23] A.B. Harris and M. Cohen, Phys. Rev. A **41**, 971 (1990).
[24] R.C. Ball and R. Blumenfeld, Phys. Rev. A **44**, 828 (1991).
[25] B. Davidovitch, M.H. Jensen, A. Levermann, J. Mathiesen, and I. Procaccia, Phys. Rev. Lett. **87**, 164101 (2001).
[26] M.B. Hastings and L.S. Levitov, Physica D **116**, 244 (1998).
[27] B. Davidovitch, H.G.E. Hentschel, Z. Olami, I. Procaccia, L.M. Sander, and E. Somfai, Phys. Rev. E **59**, 1368 (1999).
[28] B. Davidovitch, M.J. Feigenbaum, H.G.E. Hentschel, and I. Procaccia, Phys. Rev. E **62**, 1706 (2000).
[29] B. Davidovitch and I. Procaccia, Phys. Rev. Lett., **85**, 3608 (2000).
[30] B. Davidovitch, A. Levermann, and I. Procaccia, Phys. Rev. E **62**, R5919 (2000).
[31] F. Barra, B. Davidovitch, and I. Procaccia (unpublished); e-print cond-mat/0105608.
[32] Y. Hayakawa, S. Sato, and M. Matsushita, Phys. Rev. A **36**, 1963 (1987).